

# Observation of the transverse second-harmonic magneto-optic Kerr effect from Ni<sub>81</sub>Fe<sub>19</sub> thin film structures

T. M. Crawford<sup>a)</sup> and C. T. Rogers

Condensed Matter Laboratory, Department of Physics, University of Colorado at Boulder, Boulder, Colorado 80309-0390

T. J. Silva

National Institute of Standards and Technology, Boulder, Colorado 80303-3328

Y. K. Kim

Quantum Peripherals Colorado, Inc., Louisville, Colorado 80028-8188

(Received 20 October 1995; accepted for publication 9 January 1996)

We report second-harmonic magneto-optic Kerr measurements on air-exposed, polycrystalline Ni<sub>81</sub>Fe<sub>19</sub> thin films, ranging in thickness from 1 nm to 2 μm, on Al<sub>2</sub>O<sub>3</sub> coated Si (001). For samples thicker than 20 nm, in the transverse Kerr geometry, we observe a factor of 4 change in second-harmonic intensity upon magnetization reversal. For thin samples, we observe interference between second-harmonic fields from the various interfaces and deterioration of ferromagnetism in the 1 and 2 nm films. Modeling suggests that the Ni<sub>81</sub>Fe<sub>19</sub>/Al<sub>2</sub>O<sub>3</sub> interface has a larger second-order susceptibility than the air/Ni<sub>81</sub>Fe<sub>19</sub> surface. © 1996 American Institute of Physics. [S0003-6951(96)03511-6]

For magnetic systems, the second-harmonic magneto-optic Kerr effect (SH-MOKE) has recently demonstrated potential for characterizing the magnetic properties of surfaces and buried interfaces.<sup>1-5</sup> Rasing and collaborators have used multilayers of Co/Au to demonstrate SH-MOKE's interfacial specificity and have shown that the technique can be a sensitive probe of magnetic properties.<sup>2-5</sup> In this letter, we report a study of SH-MOKE in Ni<sub>81</sub>Fe<sub>19</sub>, an important material in magnetic device applications and in prototype giant magnetoresistance (GMR) multilayers. Our results demonstrate a large SH-MOKE signal for NiFe alloy systems and indicate that the technique may be of importance in characterizing the magnetic properties of buried interfaces between NiFe and other materials.

Our Ni<sub>81</sub>Fe<sub>19</sub> layers are representative of those employed in magnetic recording applications: They are polycrystalline and were fabricated by rf diode sputtering on 3 in. (001) Si substrates without intentional substrate heating, except for the 2 μm sample, which was electroplated. Substrates were precoated with 200 nm of sputtered amorphous Al<sub>2</sub>O<sub>3</sub> to remove substrate orientation effects and produce a smooth surface. The samples span a thickness range from 1 nm to 2 μm.

The experimental geometry for our SH-MOKE measurements is shown in Fig. 1. The samples are excited with a mode-locked Ti:sapphire laser tuned to operate at a wavelength of 809 nm. The laser pulse width was approximately 50 fs as measured using an autocorrelator. The beam was focused to a diameter of ~50 μm and had a peak power density at the focus of ~3 GW/cm<sup>2</sup>. The excitation beam from the laser is horizontally polarized with an extinction ratio of roughly 300:1 and passed through a half-wave plate to permit polarization rotation. The light reflecting off the sample was passed through two filters to block the fundamental beam. To detect the second-harmonic light, we use an

“IR-blind” photomultiplier tube (PMT) with a sensitivity of <1% at 809 nm.

In this letter, we describe SH-MOKE measurements in the “transverse” geometry, shown in the Fig. 1 inset. Here, the incident excitation beam is polarized with the electric field vector in the plane of incidence (*p*-polarized, shown as the *x-z* plane); the film magnetization, **M**, is saturated with an external magnetic field in the *y* direction. We verified that the SH signal from our samples is *p*-polarized with an extinction ratio of typically 50:1. The SH signal arises from the nonlinear response of the electrons to the applied field; it is mediated by a 27 component third rank tensor,  $\chi_{ijk}^{(2)}$ . In a SH-MOKE experiment, one studies how the tensor elements vary with **M**. The elements fall into two categories: elements

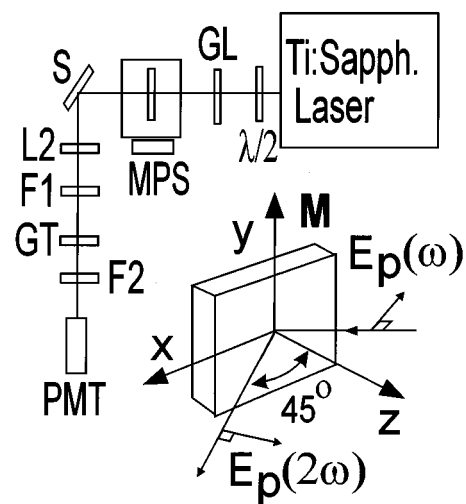


FIG. 1. Experimental setup for detecting the transverse SH-MOKE and a diagram of the sample geometry:  $\lambda/2$ =half-wave plate, GL=Glan-Taylor polarizer, L1=focusing lens, MPS=motorized positioning stage, S=sample, L2=collimating lens, F1=Ti:sapphire blocking filter, GT=Glan-Thompson polarizer, F2=405 nm interference filter, PMT=photomultiplier tube. The input light is *p* polarized, while **M** is perpendicular to the plane of incidence. We use an angle of incidence of 45°.

<sup>a)</sup>Electronic mail: crawfort@spot.colorado.edu

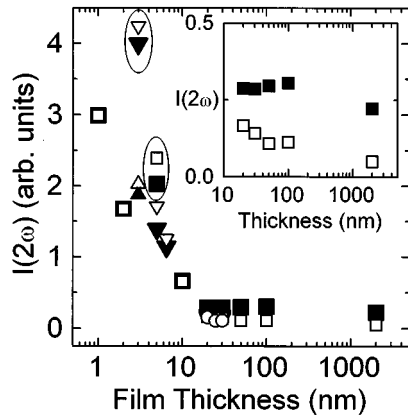


FIG. 2. SH intensity vs  $\text{Ni}_{81}\text{Fe}_{19}$  film thickness in the transverse geometry. Solid symbols show intensities with  $\mathbf{M}$  “up” while open symbols for  $\mathbf{M}$  “down.” The squares are a set of samples grown two weeks prior to measurement. The other symbols are for samples over one year old. The circled cases show unusually large SH intensity found for a few samples. Inset shows the data on an expanded scale for films thicker than the optical penetration depth.

that are unchanged by reversal of  $\mathbf{M}$  and elements that change sign upon reversal. Thus the second-harmonic intensity has terms that are invariant upon reversal of  $\mathbf{M}$  and others that change sign. The result is an  $\mathbf{M}$ -dependent intensity.

In Fig. 2, we show the detected SH intensity plotted versus  $\text{Ni}_{81}\text{Fe}_{19}$  film thickness, with the direction of  $\mathbf{M}$  as a parameter. The solid symbols in Fig. 2 were taken with  $\mathbf{M}$  pointing “up” and open symbols are for  $\mathbf{M}$  pointing “down” relative to the optical plane of incidence. We refer to the SH intensities for these cases, respectively, as  $I_+$  and  $I_-$ . The square symbols in Fig. 2 represent one set of nine samples fabricated using identical conditions approximately two weeks before these measurements were taken. The other symbols represent seven samples grown approximately one year before measurement. In Figs. 3(a) and 3(b), we show an alternative way to present the data of Fig. 2. Figure 3(a) shows the “even” symmetry component of the SH conversion efficiency  $\alpha^{\text{even}} \equiv (I_+ + I_-)/2I^2(\omega)$ , where  $I(\omega)$  is the fundamental intensity. Similarly, Fig. 3(b) shows the “odd” symmetry contributions to the SH conversion efficiency,  $\alpha^{\text{odd}} \equiv (I_+ - I_-)/2I^2(\omega)$ . In computing  $\alpha^{\text{odd}}$  and  $\alpha^{\text{even}}$  we measured quasi-static laser power and pulse width for each set of data and used these values to estimate the instantaneous power at the sample.

Several important facts are evident from Figs. 2 and 3: First, the  $\mathbf{M}$ -dependent intensity changes are very large. For films thicker than the  $\text{Ni}_{81}\text{Fe}_{19}$  optical penetration depth (roughly 15 nm), shown in expanded form in the Fig. 2 inset, we find that  $I_+$  is 3 to 4 times larger than  $I_-$ . The relative intensity change  $(I_+ - I_-)/(I_+ + I_-) = \alpha^{\text{odd}}/\alpha^{\text{even}}$ , of roughly 60% is *huge* compared with typical values of  $10^{-3}$  to  $10^{-2}$  found for linear MOKE.<sup>6</sup> The SH-MOKE signal is simple to detect and offers an easily implemented way to study Ni–Fe films. Second, we note the increase in total SH intensity and the fact that  $I_-$  becomes the “bright” state for films below 10 nm. These effects, which arise for films thinner than the optical penetration depth, are likely due to SH contributions from the buried interfaces.

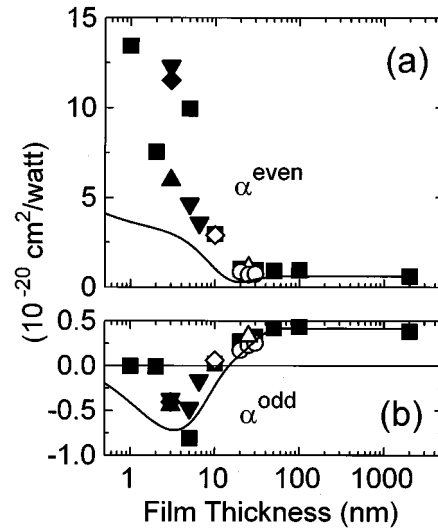


FIG. 3. Components of the SH conversion efficiency that are either even,  $\alpha^{\text{even}}$ , or odd,  $\alpha^{\text{odd}}$ , with respect to reversal of  $\mathbf{M}$ , vs film thickness. (a)  $\alpha^{\text{even}}$  vs  $\text{Ni}_{81}\text{Fe}_{19}$  film thickness. The symbol sizes indicate the variation in SH data taken on different days. The solid line is a fit to the data using the theory described in the text with tensor elements  $\chi_{XXX}^{(2)}(\text{Ni}_{81}\text{Fe}_{19}/\text{Al}_2\text{O}_3) = 2$ ,  $\chi_{XXX}^{(2)}(\text{Ni}_{81}\text{Fe}_{19}/\text{Al}_2\text{O}_3) = 5$  (both relative to the corresponding components of the air/ $\text{Ni}_{81}\text{Fe}_{19}$  interface), and  $\varphi = 75^\circ$ . The solid curve approaches the bare substrate efficiency of  $5.3 \times 10^{-20} \text{ cm}^2$ . (b)  $\alpha^{\text{odd}}$  vs  $\text{Ni}_{81}\text{Fe}_{19}$  film thickness. The solid line is a fit to the data using the theory described in the text with the same susceptibility values used in (a). It crosses zero at 15 nm due to destructive interference between SH light radiated from the air/ $\text{Ni}_{81}\text{Fe}_{19}$  and  $\text{Ni}_{81}\text{Fe}_{19}/\text{Al}_2\text{O}_3$  interfaces.

Also, we can qualitatively see the deterioration of ferromagnetism in the thinnest films: There is a small  $\mathbf{M}$ -dependent change in intensity for the 2 nm films. The  $\mathbf{M}$ -dependent signal at 1 nm is below the experimental noise floor, indicating little or no ferromagnetic response for these very thin air-exposed films. We have verified that the loss of SH-MOKE, which is consistent with the observed suppression of ferromagnetism in thin NiFe-alloy films due to oxidation,<sup>7</sup> indeed correlates with the loss of ferromagnetism, using vibrating-sample magnetometry.

This type of qualitative information regarding the existence and strength of ferromagnetic response along with the large intensity changes upon reversal of  $\mathbf{M}$  suggest that SH-MOKE can easily be applied to study any physical effect that influences  $\mathbf{M}$ . We now discuss the analysis of the data shown in Figs. 2 and 3 to provide *quantitative* information regarding  $\chi_{ijk}^{(2)}$ , and thus the interfacial magnetic properties of the  $\text{Ni}_{81}\text{Fe}_{19}$  films. Generally, the reduction of optical reflectivity data to optical susceptibility is model dependent. The success of the reduction is, therefore, dependent on how closely the model corresponds to the actual system. Our analysis assumes parallel, planar interfaces and uses tabulated bulk indices. It semiquantitatively explains the observed thickness dependence; it also illustrates the type of data reduction that is required to realize the potential of SH-MOKE for quantitatively understanding interfacial effects.

A detailed multiple reflection theory for SH-MOKE has been developed by Wierenga *et al.*<sup>8</sup> Our analysis is similar: In the model calculation, we use a transfer matrix formalism and the bulk indices of refraction [for  $\text{Ni}_{81}\text{Fe}_{19}$ ,  $n(809 \text{ nm}) = 2.59 + i4.43$ , for  $\text{Al}_2\text{O}_3$   $n(809 \text{ nm}) = 1.76$ , for

Si,  $n(809 \text{ nm}) = 3.70 + i0.008$ ]<sup>9-11</sup> to determine the fundamental fields  $\mathbf{E}_\omega^{(1)}(m)$  at each interface,  $m$ . A SH polarization  $P_{2\omega}^{(2)}(m)$  is induced by these fields via the second-order susceptibility tensor  $\chi_{ijk}^{(2)}(m)$  for each interface. These SH polarizations can then radiate second-harmonic light into the far field through a second set of transfer matrices, now evaluated at  $2\omega$  [for  $\text{Ni}_{81}\text{Fe}_{19}$ ,  $n(405 \text{ nm}) = 1.45 + i2.73$ , for  $\text{Al}_2\text{O}_3$ ,  $n(405 \text{ nm}) = 1.79$ , for Si,  $n(405 \text{ nm}) = 6.06 + i0.63$ ].<sup>9-11</sup> The SH intensity arises from field contributions generated at both  $\text{Ni}_{81}\text{Fe}_{19}$  interfaces, as well as at the  $\text{Al}_2\text{O}_3/\text{Si}$  interface. No bulk contributions to  $\chi^{(2)}$  were included in the model.

As we discussed above, the terms in  $\chi^{(2)}(n)$  are of two classes: There are terms that arise from processes independent of or even in  $\mathbf{M}$  and terms that are odd in  $\mathbf{M}$ . Within our model, the phases of these terms for the two  $\text{Ni}_{81}\text{Fe}_{19}$  interfaces differ by  $180^\circ$  due to an approximate mirror symmetry. A phase difference also exists between the even- and odd-symmetry terms. It is expected to be  $90^\circ$  in the absence of dissipation; in a real material, dissipation shifts this phase away from  $90^\circ$ .<sup>8</sup>

Finally, we used only two of the possible nonzero susceptibility elements: The first,  $\chi_{XXX}^{(2)}$ , is an odd-symmetry element, while the second,  $\chi_{ZXX}^{(2)}$ , is even.<sup>12</sup> These elements are preferentially excited because the  $x$ -directed fundamental electric fields inside the multilayer exceed the  $z$  components by roughly an order of magnitude due to refraction. We constrained the parameters to fit the  $2 \mu\text{m}$   $\text{Ni}_{81}\text{Fe}_{19}$  film, where the SH intensity arises only from the top air/ $\text{Ni}_{81}\text{Fe}_{19}$  interface, and to fit the bare  $\text{Si}/\text{Al}_2\text{O}_3$  substrate. For  $2 \mu\text{m}$   $\text{Ni}_{81}\text{Fe}_{19}$ , the experimentally determined ratio of  $\alpha^{\text{odd}}/\alpha^{\text{even}} = 0.63$ , while  $\alpha^{\text{even}}(\text{Si}/\text{Al}_2\text{O}_3)/\alpha^{\text{even}}(\text{air}/\text{Ni}_{81}\text{Fe}_{19}) = 9$ . To match these data points, we set  $\chi_{XXX}^{(2)}(\text{air}/\text{Ni}_{81}\text{Fe}_{19})/\chi_{ZXX}^{(2)} \times (\text{air}/\text{Ni}_{81}\text{Fe}_{19}) = 0.19$ , and we set  $\chi_{ZXX}^{(2)}(\text{Si}/\text{Al}_2\text{O}_3)/\chi_{ZXX}^{(2)} \times (\text{air}/\text{Ni}_{81}\text{Fe}_{19}) = 1.1$ . Little SH is generated from  $\text{Al}_2\text{O}_3$ .<sup>13</sup>

We ignore the  $\text{Al}_2\text{O}_3/\text{air}$  interface in fitting the substrate.

With these constraints at  $z=0$  and  $z=2 \mu\text{m}$ , we fitted the rest of the data with three thickness-independent parameters:  $\chi_{ZXX}^{(2)}(\text{Ni}_{81}\text{Fe}_{19}/\text{Al}_2\text{O}_3)$ ,  $\chi_{XXX}^{(2)}(\text{Ni}_{81}\text{Fe}_{19}/\text{Al}_2\text{O}_3)$ , and the relative phase shift between them,  $\varphi$ . The solid lines in Figs. 3(a) and 3(b) are fits with  $\chi_{ZXX}^{(2)}(\text{Ni}_{81}\text{Fe}_{19}/\text{Al}_2\text{O}_3) = 2$ ,  $\chi_{XXX}^{(2)}(\text{Ni}_{81}\text{Fe}_{19}/\text{Al}_2\text{O}_3) = 5$  (both relative to the corresponding element at the air/ $\text{Ni}_{81}\text{Fe}_{19}$  interface), and  $\varphi = 75^\circ$ .

The fits in Figs. 3(a) and 3(b) reproduce much of the qualitative behavior observed in the data. The quality of the fit could likely be improved by using linear ellipsometry to determine the indices of refraction at  $\omega$  and  $2\omega$  *in situ*, and by adding parameters to reflect thickness dependences of the tensor elements (see below). However, within this three-parameter model, the thickness dependence of  $\alpha^{\text{odd}}$  and  $\alpha^{\text{even}}$  arises entirely from interference between the SH fields radiated from the two  $\text{Ni}_{81}\text{Fe}_{19}$  interfaces and from the  $\text{Si}/\text{Al}_2\text{O}_3$  interface. The sign change in  $\alpha^{\text{odd}}$  at 10 nm is because  $\chi_{XXX}^{(2)}(\text{Ni}_{81}\text{Fe}_{19}/\text{Al}_2\text{O}_3)$  is  $5\times$  larger than  $\chi_{XXX}^{(2)} \times (\text{air}/\text{Ni}_{81}\text{Fe}_{19})$ . As the  $\text{Ni}_{81}\text{Fe}_{19}$  film thickness decreases, the second-harmonic polarization of the buried interface increases. The top and bottom polarizations interfere and eventually pull the odd-symmetry contribution to the intensity through 0 at 10 nm. Below 5 nm, the  $\text{Si}/\text{Al}_2\text{O}_3$  SH field is

significant. It changes from being in phase with the bottom  $\text{Ni}_{81}\text{Fe}_{19}$  field to being nearly in phase with the top  $\text{Ni}_{81}\text{Fe}_{19}$  field, thus bringing  $\alpha^{\text{odd}}$  back toward 0 with decreasing thickness.

The fitted parameters,  $\chi_{ZXX}^{(2)}$  and  $\chi_{XXX}^{(2)}$ , for the buried  $\text{Ni}_{81}\text{Fe}_{19}/\text{Al}_2\text{O}_3$  interface are, respectively, 2 and 5 times larger than their counterparts for the air/ $\text{Ni}_{81}\text{Fe}_{19}$  interface. Thus, the buried interface has better SH properties than the top interface, likely due to increased nonlinearity (sharper interface), larger  $\mathbf{M}$ , or a combination of these effects. With further modeling of the susceptibility elements, it may prove possible to determine the relative importance of these and other contributions to the nonlinear process.

Understanding the magnetic properties of Ni-Fe interfaces is important for future device applications: Modern field sensor heads, prototype Ni-Fe/Ag multilayer sensors, and spin-valve GMR materials all involve multilayers of Ni-Fe alloys and nonmagnetic spacer materials.<sup>14,15</sup> Our results for  $\text{Ni}_{81}\text{Fe}_{19}$  film structures indicate that the SH-MOKE signal in these air-exposed  $\text{Ni}_{81}\text{Fe}_{19}$  films is large and can be easily used as a qualitative measure of interfacial ferromagnetism. The quantitative determination of interfacial properties via SH-MOKE requires a thorough analysis of multilayer interference effects. With careful modeling, including a complete understanding of the linear optical properties at both  $\omega$  and  $2\omega$ , SH-MOKE could become an important technique for the quantitative study of interfaces in thin film magnetic systems.

The authors gratefully acknowledge helpful discussions with Ron Goldfarb and Steve Russek at NIST-Boulder.

- <sup>1</sup>J. Reif, J. C. Zink, C. M. Schneider, and J. Kirschner, *Phys. Rev. Lett.* **67**, 2878 (1991).
- <sup>2</sup>G. Spierings, V. Koutsos, H. A. Wierenga, M. W. J. Prins, D. Abraham, and Th. Rasing, *Surf. Sci.* **287/288**, 747 (1993).
- <sup>3</sup>G. Spierings, V. Koutsos, H. A. Wierenga, M. W. J. Prins, D. Abraham, and Th. Rasing, *J. Magn. Magn. Mater.* **121**, 109 (1993).
- <sup>4</sup>H. A. Wierenga, M. W. J. Prins, D. L. Abraham, and Th. Rasing, *Phys. Rev. B* **50**, 1282 (1994).
- <sup>5</sup>H. A. Wierenga, W. De Jong, M. W. J. Prins, Th. Rasing, R. Vollmer, A. Kirilyuk, H. Schwabe, and J. Kirschner, *Phys. Rev. Lett.* **74**, 1462 (1995).
- <sup>6</sup>D. Bonnenberg, K. A. Hempel, H. P. J. Wijn, in *Landolt-Bornstein: Numerical Data and Functional Relationships in Science and Technology*, edited by K. H. H. E. Madelung (Springer-Berlin, 1985), Vol. 19a, p. 268.
- <sup>7</sup>K. Ounadjela, H. Lefakis, V. S. Speriosu, C. Hwang, and P. S. Alexopoulos, *J. Appl. Phys.* **65**, 1230 (1988).
- <sup>8</sup>H. A. Wierenga, M. W. J. Prins, and Th. Rasing, *Physica B* **204**, 281 (1995).
- <sup>9</sup>For our  $\text{Ni}_{81}\text{Fe}_{19}$ , we used tabulated data for  $\text{Ni}_{80}\text{Fe}_{20}$  from C. L. Foiles, in *Landolt-Bornstein: Numerical Data and Functional Relationships in Science and Technology*, edited by K. H. H. E. Madelung (Springer-Berlin, 1985), Vol. 15b, p. 443.
- <sup>10</sup>F. Gervais, in *Handbook of Optical Constants of Solids II*, edited by E. F. Palik (Academic, Boston, MA, 1991), p. 761.
- <sup>11</sup>D. F. Edwards, in *Optical Constants of Solids*, edited by E. F. Palik (Academic, Boston, MA, 1985), Vol. 1, p. 552.
- <sup>12</sup>Ru-Pin Pan, H. D. Wei, and Y. R. Shen, *Phys. Rev. B* **39**, 1229 (1989).
- <sup>13</sup>A. Wokaun, J. G. Bergman, J. P. Heritage, A. M. Glass, P. F. Liao, and D. H. Olson, *Phys. Rev. B* **24**, 849 (1981).
- <sup>14</sup>T. L. Hylton, K. R. Coffey, M. A. Parker, and J. K. Howard, *Science* **261**, 1021 (1993).
- <sup>15</sup>C. Tsang, R. E. Fontana, T. Lin, D. E. Heim, V. S. Speriosu, B. A. Gurney, and M. L. Williams, *IEEE Trans. Magn.* **30**, 3801 (1994).